Terr. Atmos. Ocean. Sci., Vol. 28, No. 3, 229-238, June 2017 doi: 10.3319/TAO.2015.08.20.01(GSC)

Case study on safety index for CO_2 sequestration in a deep saline aquifer

Bieng-Zih Hsieh *, Chien-Hao Shen, Hsing-I Hsiang, and Zsay-Shing Lin

Department of Resources Engineering, National Cheng Kung University, Tainan City, Taiwan

Article history:
Received 3 March 2012
Accepted 20 August 2015

Keywords:
Carbon dioxide geological sequestration, Deep saline aquifer, Greenhouse gas emission, Numerical simulation, Plume migration, Trapping mechanism

Citation:
Hsieh, B.-Z., C.-H. Shen, H.-I. Hsiang, and Z.-S. Lin, 2017: Case study on safety index for CO_2 sequestration in a deep saline aquifer. Terr. Atmos. Ocean. Sci., 28, 229-238, doi: 10.3319/TAO.2015.08.20.01(GSC)

ABSTRACT

This study evaluates the risk for CO_2 leakage from a storage site using a risk assessment criterion, the safety index, which considers the contributions of residual gas, solubility, ionic, and mineral trapping mechanisms. We present a case of CO_2 storage in a deep saline aquifer in Yutengping (YTP) sandstone, Tiehchanshan (TCS) field, Taiwan. The numerical method was used to estimate the amount of different CO_2 phases sequestered by the various trapping mechanisms. The CO_2 injection rate was 1 million tons per year for 20 years. The total simulation time was 1000 years. In the case of down-dip well injection, the safety index was 0.77 at the storage time of 1000 years and much higher than the safety index of 0.45 for the up-dip well. More mobile supercritical CO_2 had to be sealed using a caprock in the up-dip well injection case. Injecting CO_2 using a down-dip well is a better engineering strategy because the safety index is higher.

1. INTRODUCTION

Carbon dioxide (CO_2) capture and storage (CCS) is an effective technique for reducing greenhouse gas emissions into the atmosphere. The most feasible CO_2 storage method is geological sequestration (geosequestration) (IPCC 2005).

The main types of CO_2 geosequestration are storing CO_2 in depleted oil or gas reservoirs and deep saline aquifers. CO_2 can also be used for enhanced oil recovery (CO_2-EOR), enhanced gas recovery (CO_2-EGR), and enhanced coal bed methane recovery (CO_2-ECBM). A deep saline aquifer has the maximum storage potential for CO_2 geosequestration (IPCC 2005).

Five trapping mechanisms -- structural, residual gas, solubility, ionic, and mineral trappings -- prevent CO_2 leaks from a saline aquifer (Bachu et al. 1994; Nghiem et al. 2004, 2009a; Kumar et al. 2005). Using these trapping mechanisms, CO_2 can be stored simultaneously in five different phases: mobile supercritical phase, immobile supercritical phase (residual CO_2), aqueous phase (dissolved CO_2), ionic phase (bicarbonate ions), and mineral phase (carbonates).

The risks for CO_2 leakage from the various trapping mechanisms are different. Mobile supercritical CO_2, which is trapped by the structural trapping mechanism, has the highest risk of leakage. CO_2 in immobile supercritical, aqueous, and ionic phases, which are trapped by residual gas, solubility, and ionic trapping mechanisms have a very low risk of leakage. There is no risk of leakage from the mineral trapping mechanism because CO_2 is stored as secondary carbonate minerals.

The most essential issue for a CO_2 geosequestration project is to prove that the storage is safe, which means that the injected CO_2 is expected to be permanently stored in the formation without any risk of leakage. The risk for CO_2 leakage from a storage reservoir must be evaluated to convince the public that the CO_2 is safely stored.

Nghiem et al. (2009b) used the residual gas and solubility trapping mechanisms to define the trapping efficiency index, which was used to find an optimum trapping process to reduce the risk of CO_2 leakage. However, mineral trapping, which is the safest mechanism but a slow process, was not considered in the trapping efficiency index. For a long-term risk assessment of CO_2 storage the contributions from

* *Corresponding author*
E-mail: bzhsieh@mail.ncku.edu.tw

all of the safe trapping mechanisms should be considered.

The purpose of this study was to evaluate the risk for CO_2 leakage from a storage site using a risk assessment criterion, the safety index, which considers the contributions from all of the safe trapping mechanisms. We present a CO_2 storage case in a deep saline aquifer in Yutengping (YTP) sandstone, Tiehchanshan (TCS) field, Taiwan.

2. EVALUATION OF THE SAFETY INDEX

The safety index used to evaluate the risk for CO_2 leakage is defined as follows:

$$SFI = \frac{C_r + C_d + C_i + C_m}{C_{inj}} \quad (1)$$

where SFI = the safety index, C_{inj} = the cumulative number of moles of injected CO_2 at the current time, C_r = the number of moles of the immobile supercritical CO_2 (residual gas trapping), C_d = the number of moles of the aqueous phase CO_2 (solubility trapping), C_i = the moles of the ionic phase CO_2 (ionic trapping), and C_m = the number of moles of the mineral phase CO_2 (mineral trapping).

The number of moles of CO_2 trapped by the different trapping mechanisms, which is used in Eq. (1), is dynamic and changes with time after the CO_2 has been injected. However, the conservation of mass is maintained during and after the CO_2 injection, as follows:

$$C_{inj} = C_s + C_r + C_d + C_i + C_m \quad (2)$$

where C_s = the number of moles of the mobile supercritical phase CO_2 (structural trapping).

The cumulative number of moles of injected CO_2 (C_{inj}) in Eqs. (1) and (2) were calculated from the injection rate and the injection time. The methodologies for calculating the moles of CO_2 trapped by the different trapping mechanisms are as follows.

2.1 Structural Trapping

CO_2 has a critical pressure of 7376 kPa and a critical temperature of 304.2 K (31°C). It usually becomes a supercritical fluid when injected into an aquifer below 800 m depth (Bachu et al. 1994). The density of the stored CO_2 is approximately 5160 kg m^{-3} at reservoir conditions of 13.37 Mpa and 72°C, which is lower than that of formation saline (10039 kg m^{-3} at the same reservoir conditions). The injected CO_2 migrates upward because of buoyancy and subsequently accumulates under the caprock. Thus, the structural trapping mechanism needs a caprock to prevent mobile CO_2 leaks from the storage reservoir. In this study, the CO_2 trapped from the structural trapping mechanism refers to mobile supercritical CO_2. The number of moles of CO_2 trapped by structural trapping (C_s) is calculated from the equation for the conservation of mass [Eq. (2)] when the number of moles of CO_2 trapped by residual gas, solubility, ionic, and mineral trapping is calculated.

2.2 Residual Gas Trapping

The residual gas trapping mechanism converts CO_2 into an immobile phase in the pores by the capillary effect and imbibition (Juanes et al. 2006). The classical Land's model (Land 1968) was used in this study to calculate residual gas saturation (S_{gr}), as follows (Nghiem et al. 2009b):

$$S_{gr} = S_{g,crit} + \frac{(S_{g,shift} - S_{g,crit})}{[1 + C(S_{g,shift} - S_{g,crit})]} \quad (3)$$

$$C = \frac{1}{S_{gr,\max}} - \frac{1}{S_{gt,\max}} \quad (4)$$

where S_{gr} = residual gas saturation corresponding to $S_{g,shift}$, $S_{g,shift}$ = the value of gas saturation when the shift to imbibition occurs, $S_{g,crit}$ = critical gas saturation, C = Land's coefficient, $S_{gt,\max}$ = the maximum gas saturation, $S_{gr,\max}$ = the maximum residual gas saturation.

The number of moles of CO_2 trapped by residual gas trapping (C_r) is calculated from the residual gas saturation of CO_2 (S_{gr}).

2.3 Solubility Trapping

The solubility trapping mechanism causes both mobile and immobile supercritical CO_2 to dissolve into the water (Ennis-King and Patterson 2005). CO_2 solubility in water formation (brine) was modeled as a phase-equilibrium process. The equality of the fugacities in the gas and aqueous phase was used as follows (CMG 2011):

$$f_{CO_2,g} = f_{CO_2,aq} \quad (5)$$

In this study, the fugacity of CO_2 in the gas phase ($f_{CO_2,g}$) was calculated with the Peng-Robinson equation-of-state (PR-EOS) (Peng and Robinson 1976), and the fugacity of CO_2 in the aqueous phase ($f_{CO_2,aq}$) was modeled with Henry's law (Li and Nghiem 1986), as follows:

$$f_{CO_2,aq} = y_{CO_2,aq} \cdot H_{CO_2} \quad (6)$$

where $y_{CO_2,aq}$ = the mole fraction of CO_2 in the aqueous phase, and H_{CO_2} = Henry's constant of CO_2, which is a function of pressure, temperature and salinity.

Gas solubility increases with increasing pressure and

decreases with increasing temperature or salinity. To obtain an accurate prediction of CO_2 solubility in water, this study used the correlations derived by Harvey (1996) for Henry's constants for CO_2 at the saturation pressure of H_2O and a specific temperature, the correlations developed by Bakker (2003) for the effect of salinity on Henry's constant, and a correlation developed by Garcia (2001) for the molar volume of CO_2 in water (CMG 2011).

The number of moles of CO_2 trapped by solubility trapping (C_d) is calculated from the mole fraction of CO_2 in the aqueous phase ($y_{CO_2, aq}$).

2.4 Ionic Trapping

H^+ and HCO_3^- or CO_3^{2-} ions are dissociated after the injected CO_2 dissolves in the water. The main chemical reactions related to CO_2 sequestration are as follows:

$$CO_{2(aq)} + H_2O \longleftrightarrow H^+ + HCO_3^- \tag{7}$$

$$HCO_3^- \longleftrightarrow H^+ + CO_3^{2-} \tag{8}$$

where $CO_{2(aq)}$ = the CO_2 that is dissolved in the aqueous phase (from the solubility trapping).

The chemical equilibrium reactions were used to model this reversible intra-aqueous chemical reaction (ionic trapping mechanism) in this study. The chemical equilibrium reactions were governed by chemical equilibrium constants (Bethke 1996; CMG 2011), as follows:

$$Q_\alpha - K_{eq,\alpha} = 0, \alpha = 1, ..., R_{aq} \tag{9}$$

where R_{aq} = the number of intra-aqueous chemical equilibrium reactions, $K_{eq,\alpha}$ = the chemical equilibrium constant for the aqueous reaction α, and Q_α = the activity product for the aqueous reaction α.

The $K_{eq,\alpha}$ values for aqueous reactions used here were from Kharaka et al. (1988) and Delany and Lundeen (1991). The activity product (Q_α) was calculated using (CMG 2011):

$$Q_\alpha = \prod_{k=1}^{n_{aq}} a_k^{v_{k,\alpha}} \tag{10}$$

where n_{aq} = the number of aqueous components, a_k = the component k activity, and $v_{k,\alpha}$ = the stoichiometry coefficients of the chemical equilibrium reactions.

The activities a_k are the product of the molality (m_k, moles per kg of H_2O) and the activity coefficient (γ_k) of component k. An efficient model for calculating the ionic activity coefficients is the B-dot model for the non-ideal solution (Bethke 1996) or the Pitzer (1987) model for the high-salinity solution (CMG 2011).

The number of moles of CO_2 trapped by ionic trapping (C_i) is estimated from the concentration (or molality) of bicarbonate and carbonate ions in the chemical equilibrium reactions.

2.5 Mineral Trapping

The ions that were dissociated through the chemical equilibrium reaction will react with the minerals in place and with other ions in the solution, leading to the precipitation of carbonate minerals or the dissolution of formation minerals (Gunter et al. 2004). The typical geochemical reaction for the precipitation or dissolution of Calcite ($CaCO_3$) is:

$$Calcite = H^+ \longleftrightarrow Ca^{2+} + HCO_3^- \tag{11}$$

Geochemical reactions occur between minerals and aqueous components and are reversible. The dissolution or precipitation of minerals follows the reaction rate (r_β) given by (Bethke 1996):

$$r_\beta = \widehat{A}_\beta k_\beta \left(1 - \frac{Q_\beta}{K_{eq,\beta}}\right), \ \beta = 1, ..., R_{mn} \tag{12}$$

where r_β = the reaction rate for a given mineral β, R_{mn} = the number of mineral reactions, $\widehat{A}_\beta$ = the reactive surface area, k_β = the rate constant of the mineral reaction, $K_{eq,\beta}$ = the chemical equilibrium constant of the mineral reaction, and Q_β = the activity product of the mineral reaction.

The changes in the moles of minerals through dissolution or precipitation are estimated after the geochemical reaction occurs, and then the number of moles of CO_2 trapped by mineral trapping (C_m) is estimated.

3. YTP SANDSTONE DESCRIPTION

This is a case study of CO_2 stored in an onshore deep saline aquifer. The potential storage site is YTP sandstone located in a TCS field in northwestern Taiwan (Fig. 1). The trap that was used for CO_2 storage was an anticline structure with a closure depth of 1600 meters (Fig. 1).

The YTP sandstone is the top layer of the Kueichulin (KCL) formation (Fig. 2). The depth of the YTP sandstone formation top was about 1300 m. Based on the available drilling reports, cores and well logs from the CPC Corporation, Taiwan ("Chinese Petroleum Corporation" until 2007), the YTP sandstone formation thickness was 205 m, the porosity was 0.2, and the permeability was 300 mD (Table 1).

The YTP sandstone is overlaid by Chinshui (CS) shale, which is the 300 m thick caprock of the storage reservoir (Fig. 2). The Shihliufen (SLF) shale, which is in the KCL formation, was assumed to be the lower no-flow boundary

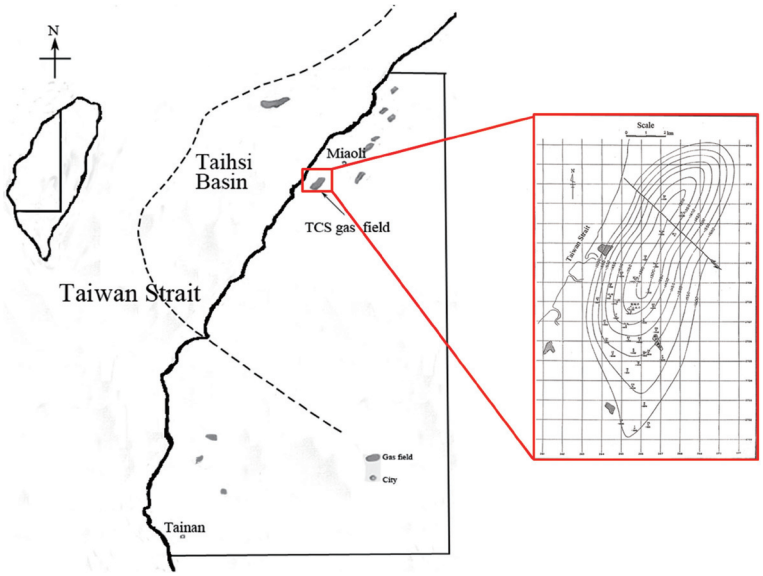

Fig. 1. The location of the TCS field in NW Taiwan (left); the anticline structure map of the YTP sandstone in the TCS field (right). (Color online only)

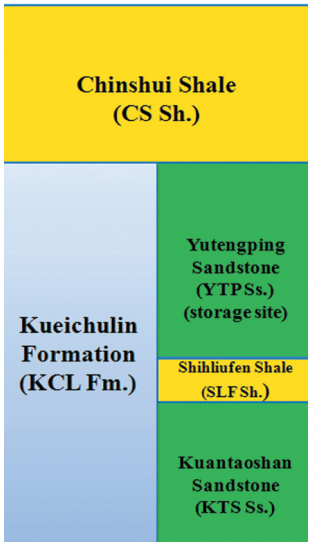

Fig. 2. The formation stratigraphy for the studied interval in the TCS field. (Color online only)

Table 1. Basic formation parameters of the YTP sandstone.

Parameter (unit)	Value
Formation Top (m)	1300
Porosity (frac.)	0.2
Thickness (m)	205
Permeability (mD)	300
Initial pressure (Mpa)	13.37
Reference depth for initial pressure (m)	1300
Temperature (°C)	72
Salinity (mg L^{-1})	16000

for this case study (Fig. 2).

4. RESERVOIR SIMULATION MODEL DEVELOPMENT

The numerical method was used in this work to study the amount of CO_2 sequestered in the deep saline aquifer using the various trapping mechanisms. The GEM compositional simulator with the GEM-GHG module was used (CMG 2011). GEM is an advanced general equation-of-state compositional simulator that models the flow of three-phase, multi-component fluids and is a certified commercial simulator in the petroleum industry for modeling the oil and gas recovery process and CO_2 storage where effective fluid composition is important (CMG 2011). GEM-GHG is a reactive transport module for modeling simultaneous geochemical reactions after CO_2 has been injected into an aquifer.

The numerical geological model was developed by dividing the anticline structure of the YTP sandstone into grids. The size of the model was about 7.5 × 13.5 km. The structure was divided to 33 × 59 × 5 grids, in which 6360 grids were active. The dimensions of each grid were 229 × 229 × 41 m.

The initial pressure of the YTP sandstone was 13.37 Mpa at the reference depth of 1300 m (Table 1). The reservoir temperature was 72°C and the water salinity was 16000 mg L^{-1}. The aquifer was assumed to be an open system with constant-pressure boundary condition in the outer boundary grids.

The drainage relative permeability curves used in this study were from the Corey correlation (Corey 1954):

$$k_{rg}(S_w) = k_{rg}^0 \left(\frac{S_g - S_{g,crit}}{1 - S_{w,crit} - S_{g,crit}} \right)^{N_g} \quad (13)$$

$$k_{rw}(S_w) = k_{rw}^0 \left(\frac{S_w - S_{w,crit}}{1 - S_{w,critc}} \right)^{N_w} \quad (14)$$

where $k_{rg}(S_w)$ = relative permeability to gas (CO_2) for the given water saturation (S_w), $k_{rw}(S_w)$ = relative permeability to water for the given water saturation, k_{rg}^0 = gas relative permeability at the maximum gas saturation ($S_{gt,\max}$), k_{rw}^0 = water relative permeability at the maximum water saturation ($S_{wt,\max}$), S_g = gas saturation, S_w = water saturation, $S_{g,crit}$ = critical gas saturation, $S_{w,crit}$ = critical water saturation, N_g = empirical parameter for gas relative permeability, and N_w = empirical parameter for water relative permeability.

The following values were assumed: gas relative permeability (k_{rg}^0) = 1.0 at the maximum gas saturation ($S_{gt,\max}$) of 0.8, water relative permeability (k_{rw}^0) = 1.0 at the maximum water saturation ($S_{wt,\max}$) of 1.0, critical gas saturation ($S_{g,crit}$) = 0.03, critical water saturation ($S_{w,crit}$) = 0.2, the empirical parameter for gas relative permeability (N_g) = 2.4, and the empirical parameter for water relative permeability (N_w) = 2.3.

For the imbibition relative permeability curve of gas, the maximum residual gas saturation ($S_{gr,\max}$) was assumed to be 0.4. The Land's coefficient (C), which is calculated from Eq. (4), was applied to the Land's model [Eq. (3)] to calculate the residual gas saturation and the imbibition relative permeability curve of gas. The imbibition relative permeability curve of water was assumed as identical to the drainage curve of the water (Juanes et al. 2006).

The composition and the molality of the formation water species were analyzed from water samples that were collected from the CPC Corporation, Taiwan (Table 2). The volume percentage of rock minerals was analyzed from rock samples using XRF (X-ray fluorescence) and XRD (X-ray diffraction) (Table 3). Based on the analyzed formation water and rock minerals results (Tables 2 and 3), we considered five intra-aqueous chemical reactions and four geochemical mineral reactions to simulate the ionic and mineral trappings (Table 4).

This study was simulated to inject 1 million tons per year of CO_2 for a period of 20 years. Cases of CO_2 injected from up-dip and down-dip wells were studied (Fig. 3). The down-dip and up-dip well locations, in terms of x and y grid numbers, were (24, 46) and (19, 24), respectively. The total simulation time was 1000 years and the long-term storage of different phases of CO_2 trapped by different trapping mechanisms in a saline aquifer was studied.

5. RESULTS AND DISCUSSION

For the case of the injection well located at the down-dip (Fig. 3), the percentage of CO_2 trapped by the structural trapping mechanism (that is, the percentage of mobile supercritical CO_2) was markedly high during the CO_2 injection period (Fig. 4, Table 5). However, the percentage of CO_2 trapped by the structural trapping mechanism decreased dramatically, from 80.77 - 23.29%, during the post-injection period because of the formation of residual CO_2 (immobile supercritical CO_2). In the post-injection period, imbibition caused a massive quantity of residual CO_2 to form behind the moving CO_2 plume when it migrated toward the structure up-dip from the injection site located at the down-dip.

The percentage of CO_2 trapped by the residual gas trapping mechanism was very low (3.65%) during the CO_2 injection period because drainage was the dominate phenomenon when CO_2 was continuously injected into the aquifer (Fig. 4, Table 5). During the post-injection period, imbibition occurred behind the migrating plume and the percentage of CO_2 trapped by the residual gas trapping mechanism increased markedly to 40.44% at the simulation time of 100 years (Fig. 4, Table 5). Subsequently, the percentage gradually decreased to 2.95% at 1000 years because the immobile supercritical CO_2 dissolved into the water.

Table 2. Molality of major species of formation water.

Species	Molality
H^+	2.64E-09
Al^{3+}	2.32E-11
Ca^{2+}	5.46E-05
$SiO_{2(aq)}$	2.38E-04
K^+	2.85E-04
HCO_3^-	1.27E-02
CO_3^{2-}	9.83E-04

Table 3. Volume percentage of minerals in formation rock.

Mineral	Volume Percentage
Quartz (SiO_2)	76.5%
Anorthite ($CaAl_2Si_2O_8$)	0.9%
Kaolinite [$Al_2Si_2O_5(OH)_4$]	0.8%
Muscovite [$KAl_3Si_3O_{10}(OH)_2$]	1.8%

Table 4. Major intra-aqueous chemical reactions and geochemical mineral reactions considered in this study.

Chemical and Mineral Reactions
Intra-aqueous chemical reactions
$CO_{2(aq)} + H_2O \longleftrightarrow H^+ + HCO_3^-$
$CO_3^{2-} + H^+ \longleftrightarrow HCO_3^-$
$OH^- + H^+ \longleftrightarrow H_2O$
$Al(OH)^{2+} + H^+ \longleftrightarrow Al^{3+} + H_2O$
$KOH + H^+ \longleftrightarrow H^+ + H_2O$
Geochemical mineral reactions
$Calcite + H^+ \longleftrightarrow Ca^{2+} + HCO_3^-$
$Anorthite + 8H^+ \longleftrightarrow 4H_2O + Ca^{2+} + 2Al^{3+} + 2SiO_{2(aq)}$
$Kaolinite + 6H^+ \longleftrightarrow 5H_2O + 2Al^{3+} + 2SiO_{2(aq)}$
$Muscovite + 6H^+ \longleftrightarrow 6H_2O + K^+ + 3Al^{3+} + 3SiO_{2(aq)}$

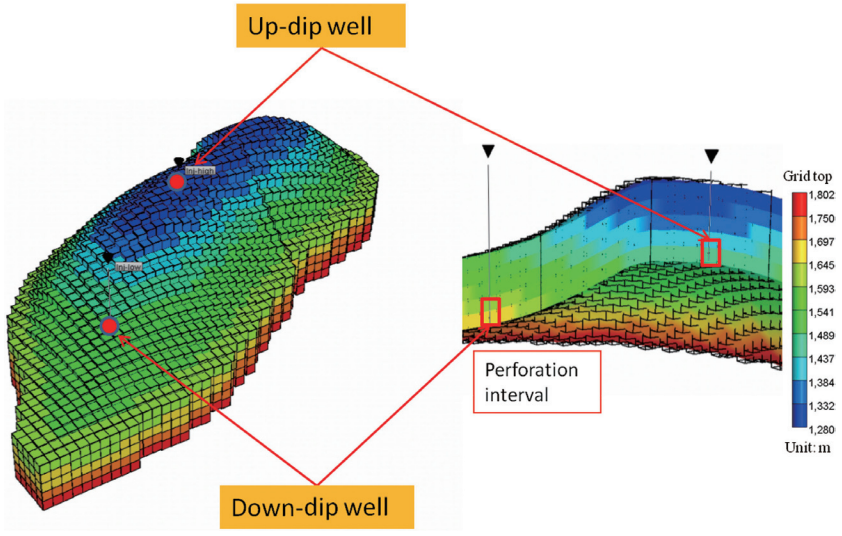

Fig. 3. The well location and perforation interval for the up-dip and down-dip wells. (Color online only)

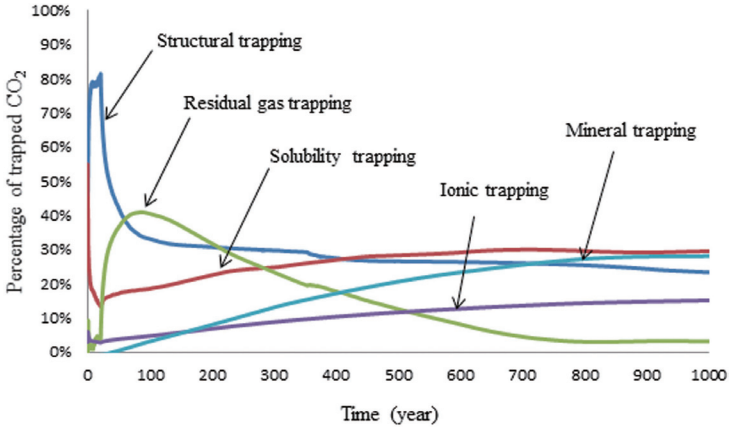

Fig. 4. The percentage of CO_2 trapped using various trapping mechanisms for the down-dip injection case. (Color online only)

Table 5. Percentage of CO_2 trapped using various trapping mechanisms in down-dip injection case.

Years	Structural Trapping Mechanism	Residual Gas Trapping Mechanism	Solubility Trapping Mechanism	Ionic Trapping Mechanism	Mineral Trapping Mechanism
10	77.95%	2.63%	16.46%	2.77%	0.03%
20	80.77%	3.65%	13.05%	2.25%	0.11%
50	42.09%	36.53%	17.11%	3.72%	0.39%
100	33.09%	40.44%	18.49%	4.66%	3.07%
300	29.71%	23.33%	24.77%	8.73%	13.02%
500	26.52%	12.54%	28.26%	11.59%	20.56%
800	25.35%	3.08%	29.50%	14.28%	27.20%
1000	23.29%	2.95%	29.55%	15.08%	28.04%

The percentage of CO_2 trapped by the solubility trapping mechanism was the second highest throughout the CO_2 injection duration, but it decreased from 16.46% at 10 years to 13.05% at 20 years (Fig. 4, Table 5). The defined calculation equation was the reason for the decreasing percentage. The equation for calculating the percentage of trapped CO_2 by an individual trapping mechanism was the amount of CO_2 trapped by an individual trapping mechanism divided by the amount of cumulative CO_2 injected. During the CO_2 injection period the amount of cumulative CO_2 injected changed over time (that is, it was not a fixed amount), which caused a decrease in the calculated percentage of trapped CO_2 from the solubility trapping, even though the amount of CO_2 trapped by the solubility trapping mechanism increased. During the post-injection period the percentage of CO_2 trapped by the solubility trapping mechanism increased gradually and reached 29.55% at 1000 years (the end of the simulation time).

The trend for the percentage of CO_2 trapped by the ionic trapping mechanism is similar to that for solubility trapping; the percentage decreased slightly from 2.77% at 10 years to 2.25% at 20 years, and then gradually increased to 15.08% at 1000 years (Fig. 4, Table 5). Almost no $CaCO_3$ precipitated during the CO_2 injection period (Table 5). However, the percentage of CO_2 trapped by the mineral trapping mechanism reached 28.04% at the simulation time of 1000 years in the post-injection period.

The safety index for evaluating the risk for leakage, which changed with time, was calculated from the safe trapping mechanisms [Eq. (1)]. The risk evaluation diagram was plotted based on the safety index calculations (Fig. 5). For the injection well located at the down-dip case, the safety index was 0.19 at the end of CO_2 injection. In the post-injection period, the safety indices were 0.58, 0.67, 0.73, and 0.77 at the storage times of 50, 100, 500, and 1000 years (Fig. 5).

For the injection well located at the up-dip case (Fig. 3), the percentage of CO_2 trapped by the structural trapping mechanism was very high (up to 87.01%) during the CO_2 injection period, but gradually declined to 54.65% during the post-injection period because of the formation of some residual CO_2 (Fig. 6, Table 6). The distance of CO_2 plume migration is a crucial factor for the formation of residual CO_2 that may affect the percentage of CO_2 trapped by the structural trapping mechanism. In the post-injection period in the up-dip injection case, the CO_2 plume migration distance was short and the plume was quickly limited

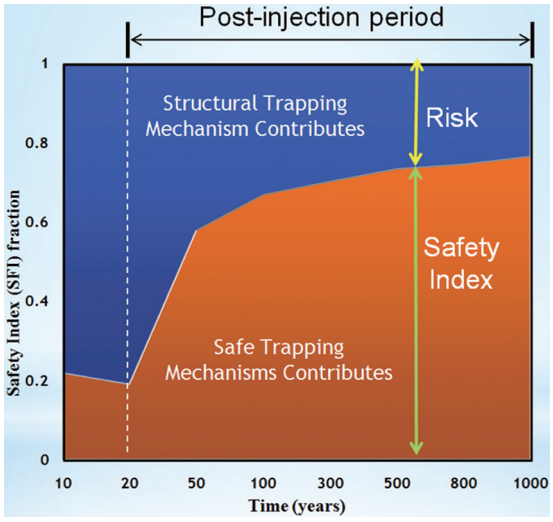

Fig. 5. The risk evaluation diagram for the down-dip injection case. (Color online only)

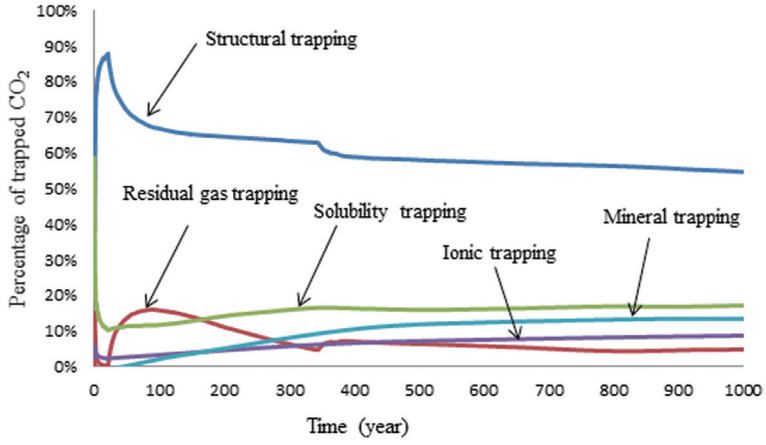

Fig. 6. The percentage of CO_2 trapped using various trapping mechanisms for the up-dip injection case. (Color online only)

Table 6. Percentage of CO_2 trapped using various trapping mechanisms in up-dip injection case.

Years	Structural Trapping Mechanism	Residual Gas Trapping Mechanism	Solubility Trapping Mechanism	Ionic Trapping Mechanism	Mineral Trapping Mechanism
10	84.65%	0.73%	11.93%	2.54%	0.01%
20	87.01%	0.29%	10.43%	2.05%	0.08%
50	71.84%	13.67%	11.37%	2.72%	0.26%
100	66.83%	15.80%	11.70%	3.30%	2.14%
300	63.32%	6.40%	15.99%	5.76%	8.11%
500	58.01%	6.38%	15.97%	7.19%	11.85%
800	56.31%	4.83%	17.17%	8.23%	13.21%
1000	54.65%	4.40%	16.91%	8.70%	13.41%

in the anticline up-dip. A small amount of residual CO_2 was formed and this caused the percentage of CO_2 trapped by the structural trapping mechanism to remain at the high level of 54.65% at the simulation time of 1000 years.

In the post-injection period the percentage of CO_2 trapped by the residual gas trapping mechanism increased from 0.29% at the end of the injection period (20 years) to 15.80% at the simulation time of 100 years (Fig. 6, Table 6). It then decreased to 4.40% at 1000 years because the residual CO_2 dissolved into the water.

The percentage of trapped CO_2 from the solubility trapping mechanism was the second highest throughout the CO_2 injection duration, but it decreased slightly from 11.93% at 10 years to 10.43% at 20 years (Fig. 6, Table 6). During the post-injection period, the percentage of trapped CO_2 from the solubility trapping mechanism increased to 16.91% at 1000 years.

The trend in the CO_2 percentage trapped by the ionic trapping mechanism was similar to that of solubility trapping. The percentage decreased slightly from 2.54% at 10 years to 2.05% at 20 years and then increased to 8.70% at 1000 years (Fig. 6, Table 6). There was no $CaCO_3$ precipitated during the CO_2 injection period. The percentage of CO_2 trapped by the mineral trapping mechanism increased to 13.41% at the simulation time of 1000 years in the post-injection period (Fig. 6, Table 6).

For the injection well located at the up-dip case, the safety index was 0.13 at the end of CO_2 injection. In the post-injection period, the safety indices were 0.28, 0.33, 0.42, and 0.45 at the storage times of 50, 100, 500, and 1000 years, respectively (Fig. 7).

The safety index [Eq. (1)] shows that the higher the percentage of CO_2 trapped by the safe trapping mechanisms, the safer the CO_2 sequestration. In other words, the higher the safety index, the lower the risk for CO_2 leakage.

Based on the results from our studied cases when CO_2 was injected using a down-dip well, the percentage of mobile supercritical CO_2, which has a high risk of leakage, decreased dramatically during the post-injection period because of the safe trapping mechanisms. However, in the case of an up-dip well, the percentage of mobile supercritical CO_2 remained at a high level after CO_2 injection because no notable residual CO_2 was formed in the early post-injection period.

In this case study for CO_2 stored in the YTP sandstone, at the end of 1000 years simulation time the safety index, which was the risk assessment criterion, was 0.77 for down-dip injection and 0.45 for up-dip injection. The amount of mobile supercritical CO_2, which must be sealed by a caprock, was greater when the up-dip well was used. Based on the safety index estimations, the better engineering strategy for this CO_2 storage case was to inject CO_2 using a down-dip well because the risk for CO_2 leakage was lower when the down-dip well was used.

6. CONCLUSIONS

The safety index is the ratio of total moles of residual, aqueous, ionic and mineral phases of CO_2 to the cumulative moles of injected CO_2 at the current time, which can be used as a risk assessment criterion to evaluate the risk for CO_2 leakage when CO_2 is stored in a deep saline aquifer.

The long-term storage of different phases of CO_2 in a deep saline aquifer from the various trapping mechanisms can be estimated using the numerical method. The CO_2 case stored in an YTP sandstone saline aquifer in a TCS field was simulated.

The CO_2 plume migration is a crucial factor for the formation of residual CO_2 that will affect the amount of high-risk mobile supercritical CO_2 in the post-injection period. When using an up-dip injection well the CO_2 plume

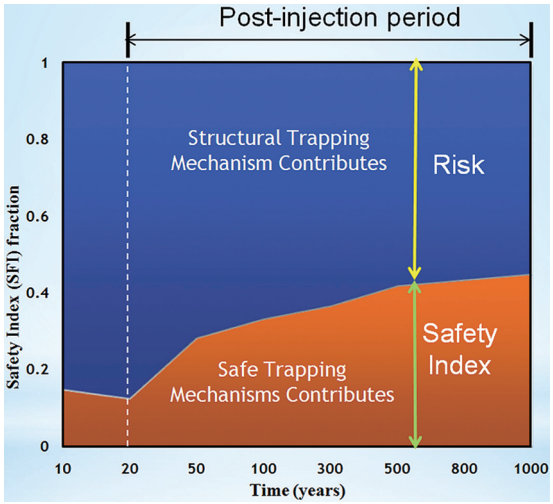

Fig. 7. The risk evaluation diagram for the up-dip injection case. (Color online only)

might be quickly limited in the anticline up-dip, which is unfavorable to CO_2 storage safety because only a small amount of residual CO_2 will be formed.

The safety index for using a down-dip well is much higher than that using an up-dip well. The amount of mobile supercritical CO_2 that must be sealed by a cap-rock was higher when an up-dip well was used. Better engineering strategy for storing CO_2 in the YTP sandstone is to inject CO_2 from a down-dip well because the higher safety index means a smaller risk for CO_2 leakage.

Acknowledgements This research was supported by grant MOST 105-3113-E-008-009 from the Taiwan Ministry of Science and Technology, National Energy Program (NEP). We especially thank the researchers and engineers from the CPC Corporation, Taiwan for their help and invaluable discussions.

REFERENCES

Bachu, S., W. D. Gunter, and E. H. Perkins, 1994: Aquifer disposal of CO_2: Hydrodynamic and mineral trapping. *Energ. Convers. Manage.*, **35**, 269-279, doi: 10.1016/0196-8904(94)90060-4. [Link]

Bakker, R. J., 2003: Package FLUIDS 1. Computer programs for analysis of fluid inclusion data and for modelling bulk fluid properties. *Chem. Geol.*, **194**, 3-23, doi: 10.1016/S0009-2541(02)00268-1. [Link]

Bethke, C. M., 1996: Geochemical Reaction Modeling: Concepts and Applications, Oxford University Press, New York, 414 pp, doi: 10.1093/petroj/38.7.971-a. [Link]

Computer Modeling Group (CMG), 2011: User's Guide GEM: Advanced Compositional Reservoir Simulator, Version 2011, Calgary, Alberta, Canada: Computer Modeling Group Ltd.

Corey, A. T., 1954: The interrelation between gas and oil relative permeabilities. *Producers Mon.*, **19**, 38-41.

Delany, J. M. and S. R. Lundeen, 1991: The LLNL thermochemical data base—revised data and file format for the EQ3/6 package. Lawrence Livermore National Laboratory Report, UCRL-21658.

Ennis-King, J. P. and L. Patterson, 2005: Role of convective mixing in the long-term storage of Carbon Dioxide in deep saline formations. *SPEJ*, **10**, 349-356, doi: 10.2118/84344-PA. [Link]

Garcia, J. E., 2001: Density of aqueous solutions of CO_2. Lawrence Berkeley National Laboratory, 1-9.

Gunter, W. D., S. Bachu, and S. M. Benson, 2004: The role of hydrogeological and geochemical trapping in sedimentary basins for secure geological storage of Carbon Dioxide. *Geol. Soc. Lond. Spec. Publ.*, **233**, 129-145, doi: 10.1144/GSL.SP.2004.233.01.09. [Link]

Harvey, A. H., 1996: Semiempirical correlation for Henry's constants over large temperature ranges. *AIChE J.*, **42**, 1491-1494, doi: 10.1002/aic.690420531. [Link]

IPCC, 2005: Special Report on Carbon Dioxide Capture and Storage, Cambridge University Press, Cambridge, United Kingdom and New York, USA, 442 pp.

Juanes, R., E. J. Spiteri, F. M. Orr Jr., and M. J. Blunt, 2006: Impact of relative permeability hysteresis on geological CO_2 storage. *Water Resour. Res.*, **42**, W12418, doi: 10.1029/2005WR004806. [Link]

Kharaka, Y. K., W. D. Gunter, P. K. Aggarwal, E. H. Perkins, and J. D. Debraal, 1988: SOLMINEQ. 88: A computer program for geochemical modeling of water-rock interactions. Water-Resources Investigations Report, No. 88-4227, U.S. Geological Survey, Menlo Park, California.

Kumar, A., M. H. Noh, G. A. Pope, K. Sepehrnoori, S. L. Bryant, and L. W. Lake, 2005: Simulating CO_2 storage in deep saline aquifers. In: Thomas, D. C. (Ed.), Carbon Dioxide Capture for Storage in Deep Geologic Formations: Results from the CO_2 Capture Project, Vol. 2, Elsevier, London, UK, 877-896, doi: 10.1016/B978-008044570-0/50140-9. [Link]

Land, C. S., 1968: Calculation of imbibition relative permeability for two- and three-phase flow from rock properties. *Soc. Pet. Eng. J.*, **8**, 149-156, doi: 10.2118/1942-PA. [Link]

Li, Y. K. and L. X. Nghiem, 1986: Phase equilibria of oil, gas and water/brine mixtures from a cubic equation of state and Henry's law. *Can. J. Chem. Eng.*, **64**, 486-496, doi: 10.1002/cjce.5450640319. [Link]

Nghiem, L. X., P. Sammon, J. Grabenstetter, and H. Ohkuma, 2004: Modeling CO_2 storage in aquifers with a fully-coupled geochemical EOS compositional simulator. SPE/DOE Symposium on Improved Oil Recovery, SPE-89474-MS, Society of Petroleum Engineers, 22-26, doi: 10.2118/89474-MS. [Link]

Nghiem, L. X., V. K. Shrivastava, D. Tran, B. F. Kohse, M. S. Hassam, and C. Yang, 2009a: Simulation of CO_2 storage in saline aquifers. SPE/EAGE Reservoir Characterization and Simulation Conference, SPE-125848-MS, Society of Petroleum Engineers, doi: 10.2118/125848-MS. [Link]

Nghiem, L. X., C. Yang, V. K. Shrivastava, B. F. Kohse, M. S. Hassam, D. Chen, and C. Card, 2009b: Optimization of residual gas and solubility trapping for CO_2 sequestration in saline aquifers. SPE Reservoir Simulation Symposium, SPE 119080, Society of Petroleum Engineers, doi: 10.2118/119080-MS. [Link]

Peng, D. Y. and D. B. Robinson, 1976: A new two-constant equation of state. *Ind. Eng. Chem. Fundam.*, **15**, 59-64, doi: 10.1021/i160057a011. [Link]

Pitzer, K. S., 1987: A thermodynamic model for aqueous solutions of liquid-like density. *Rev. Mineral. Geochem.*, **17**, 97-142.